Received: 19 February 2022 | Revised: 8 April 2022 | Accepted: 26 April 2022

DOI: 10.1002/mp.15690

REVIEW ARTICLE

MEDICAL PHYSICS

Nuclear-medicine probes: Where we are and where we are going

Andrea Gonzalez-Montoro[1] | **Cesar David Vera-Donoso**[2] | **Georgios Konstantinou**[5] | **Pablo Sopena**[3] | **Manolo Martinez**[2] | **Juan Bautista Ortiz**[2] | **Montserrat Carles**[4] | **Jose Maria Benlloch**[1] | **Antonio Javier Gonzalez**[1]

[1]Instituto de Instrumentación para Imagen Molecular (I3M), Centro Mixto CSIC Universitat Politècnica de València, Valencia, Spain

[2]Urology Department, La Fe Hospital, Valencia, Spain

[3]Servicio de Medicina Nuclear, Área clínica de Imagen Médica, La Fe Hospital, Valencia, Spain

[4]Biomedical Imaging Research Group, La Fe Hospital, Valencia, Spain

[5]Multiwave Metacrystal S.A., Geneva, Switzerland

Correspondence
Andrea Gonzalez-Montoro, Instituto de Instrumentación para Imagen Molecular (I3M), Centro Mixto CSIC Universitat Politècnica de València, Camino de Vera s/n, Ed. 8B, Acc. N, Niv. 0, 46022 Valencia, Spain.
Email: andrea.gm@i3m.upv.es

Funding information
GVA; Conselleria de Cultura, Educación y Ciencia, Generalitat Valenciana, Grant/Award Number: VALi+d Program; Fundación para la Investigación del Hospital Universitari La Fe, Grant/Award Number: IIS-F-PG-22-02

Abstract

Nuclear medicine probes turned into the key for the identification and precise location of sentinel lymph nodes and other occult lesions (i.e., tumors) by using the systemic administration of radiotracers. Intraoperative nuclear probes are key in the surgical management of some malignancies as well as in the determination of positive surgical margins, thus reducing the extent and potential surgery morbidity.

Depending on their application, nuclear probes are classified into two main categories, namely, counting and imaging. Although counting probes present a simple design, are handheld (to be moved rapidly), and provide only acoustic signals when detecting radiation, imaging probes, also known as cameras, are more hardware-complex and also able to provide images but at the cost of an increased intervention time as displacing the camera has to be done slowly.

This review article begins with an introductory section to highlight the relevance of nuclear-based probes and their components as well as the main differences between ionization- (semiconductor) and scintillation-based probes. Then, the most significant performance parameters of the probe are reviewed (i.e., sensitivity, contrast, count rate capabilities, shielding, energy, and spatial resolution), as well as the different types of probes based on the target radiation nature, namely: gamma (γ), beta (β) (positron and electron), and Cherenkov. Various available intraoperative nuclear probes are finally compared in terms of performance to discuss the state-of-the-art of nuclear medicine probes.

The manuscript concludes by discussing the ideal probe design and the aspects to be considered when selecting nuclear-medicine probes.

KEYWORDS
intraoperative instruments, nuclear medicine, nuclear probes, radiation detectors

1 | INTRODUCTION

Cancer, in its broadest sense, refers to around 280 different types of disease and is the result of genetic and other changes that lead to cellular dysfunctions.[1] Cancer constitutes one of the leading causes of death worldwide; thus, its early diagnosis and assessment after surgery constitute a major global concern. During 2020, more than 19 million new cancer cases were diagnosed causing approximately 10 million deaths. By 2040, these numbers are estimated to reach 29.5 million and 16.4 million, respectively.[2]

Depending on the cancer stage when is first diagnosed, different treatment methodologies are available. The possibility of surgical intervention usually increases survival rates,[3] being surgical resection the preferred option for localized tumors in patients whose organ is still functional.[4] The high mortality rate of some cancers

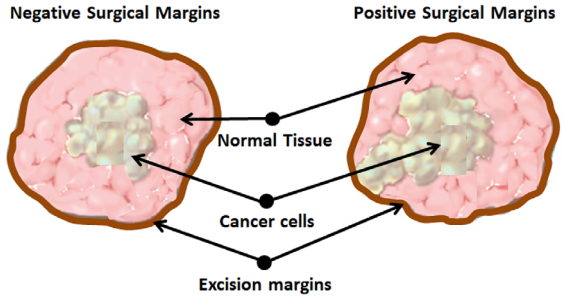

FIGURE 1 Illustrative drawing of negative and positive surgical margins

relates to the long-term outcomes after surgery that are influenced by factors such as the number and size of tumoral cells, presence of cancer in the vascular system, and remaining positive surgical margins (PSM).[5]

A surgical margin, also called resection margin, is the boundary of seemingly noncancerous cells where the malignancy has been surgically removed. The excised specimen is microscopically examined by a pathologist to check if the surgical margin is free from cancerous cells and, if cancerous cells are found at these boundaries, that is, PSM, then it is unlikely that the surgery achieves good results, and the patient will probably need another intervention or adjuvant treatments such as radiation therapy with increased morbidity or complications on their health. Figure 1 provides a sketch showing the difference between negative and PSM. The presence of PSM is a foremost problem after resection surgeries and the main cause of cancer persistence and recurrence.[5–7] Note that PSMs are present in all cancer types requiring the removal of a tumor or tissue (special relevant in prostate[8] and kidney cancers[9]); thus, its precise identification is a common requirement.

In addition to conventional methods looking at thin slices of excised tissue from the boundaries of the resection margin, methods based on intraoperative imaging techniques are used to assess PSM[10] in real time; thus, in the case of a positive outcome, the correction can be made during the same intervention. However, the accuracy of these techniques is limited,[11] resulting in false negatives and causing the recurrence of cancer at the surgical margin.

To improve the delimitation of surgical margins, alternative approaches have been suggested. The use of intraoperative tools for both surgery and therapy guidance has become crucial in this regard as it allows one to mitigate the errors associated with reduced quantitative information available during surgery. Different intraoperative counting and imaging modalities are currently used, each one has different applications depending on the sensitivity, spatial capabilities, timing resolution, and field of view (FOV) required. Table 1 outlines the most common used techniques and their main features.

Among these techniques, nuclear medicine has proven to be the ideal candidate for the determination of PSM[8] and, in particular, handheld counting or imaging nuclear probes have been demonstrated to be key instruments[11,12] as they allow the surgeon to easily identify the presence of radioactivity (after the injection of a radiotracer usually for presurgery imaging of the lesion) by slowly displacing the probe over the excised area. Sketches of 1D nuclear probes used for different purposes are shown in Figure 2.

In the following, the different intraoperative probes used in nuclear medicine and their applications are summarized. Moreover, a comprehensive description of the different types of probes, including counting and imaging devices, as well as the materials and methodology most commonly used, is presented. The manuscript concludes with a description of what we consider the "ideal probe."

2 | NUCLEAR MEDICINE PROBES

The first reported use of intraoperative probes dates from 1951[14] and since then, the numbers of applications and manufacturers offering commercial intraoperative probes have exponentially grown. The evolution and development of high-performance and high-sensitivity probes has been closely tied to the progress in high-performance detector technology and advancements in scintillation materials.

Intraoperative probes are used in general for the detection of the radiation that usually results from the injection (or eventually inhalation or swallowing) of a radiotracer compound and, in particular, for sentinel lymph node (SLN) biopsy.[15] Nuclear medicine probes are used as a complementary tool for a more precise location of malignancies either to guide biopsy procedures or for their removal in the surgical field (SLN or residual tumoral cells).

As will be discussed later, probes can be designed to directly detect beta (β) particles (superficial detection) or gamma (γ) rays (deep detection).[16] In the case of beta emitters, the positron annihilates with an orbital electron in the patient's tissue emitting as a result two opposed 511-keV γ-rays (depending on the probe's design and application either the positron or annihilation radiation is detected), but, in the case of single gamma radiotracers (scintigraphic), a gamma particle is directly emitted and detected.[14]

In general, probes are classified into two main categories based on the complexity of the design, namely, counting or imaging (i.e., gamma cameras) probes. Counting probes provide only variable acoustic signals corresponding to the rate of detected radiation and are handheld enabling fast movements of the probe across the surface under evaluation. Moreover, counting probes are exposed to biological fluids (e.g., blood); thus, the probe's head must be waterproof. Imaging probes, however, are able to provide images that are useful

TABLE 1 Main features of commonly used intraoperatively techniques

Modality	Spatial resolution	Temporal resolution	FOV (mm)	Cost ($)	Enhanced tissue
US	~μm	~120 frame/s	~200	10–100k	Muscles, tendons, ligaments, and vessels
X-ray	μm mm	~7–30	~430	10–100k	Bones and vessels
OCT	μm	~4–40	~200	10–100k	Cytoarchitecture
MR	mm	~5–15	~550	1–10M	Muscles, tendons, ligaments, vessels, and metabolic and functional processes
Endo/laparoscopy	μm m	~10–30	~100	0.1–100k	Bones, muscles, tendons, ligaments, vessels, and metabolic and functional processes
PA imaging	μm m	<0.01	~100	1–10k	Bones, vessels, and metabolic and functional processes
Nuclear medicine	~*mm*	<0.01	~5	10–500k	Metabolic and functional processes
Raman spectroscopy	<*mm*	<0.01	~200	10–100k	Cytoarchitecture

Abbreviations: FOV, field of view; MR, magnetic resonance; OCT, optical coherence tomography; PA, photoacoustic; US, ultrasounds.

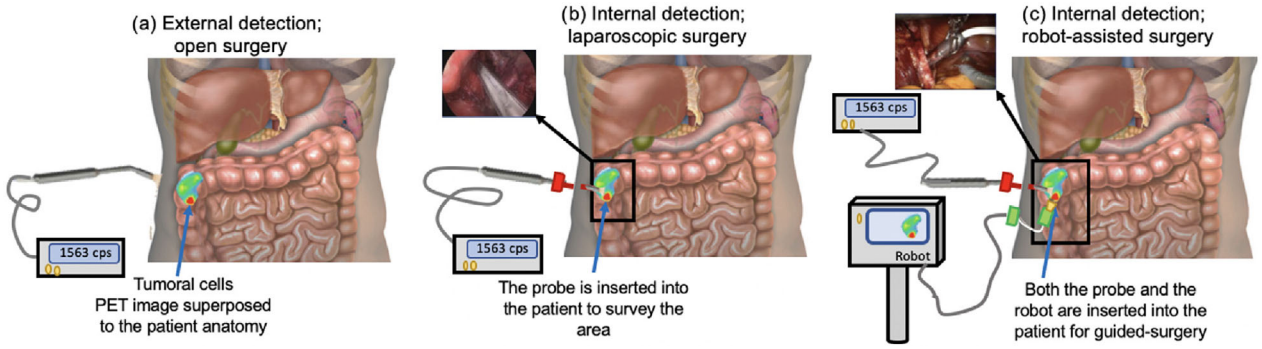

FIGURE 2 Sketches of 1D nuclear detection probes: (a) external detection of tumoral cells during open intervention operating with a gamma probe, (b) internal detection during surgery with a gamma probe, and (c) internal detection during robot-assisted surgery. Real surgical pictures extracted from Ref. [13]

for guiding biopsy. Providing accurate images usually requires adding collimators at the entrance face of the probe's detector. Collimators allow identifying the source of radiation emission while reducing the contribution of radiation coming from surrounding areas (noise). However, collimators are bulky and heavy thus the movement of imaging probes is limited and slow. Moreover, including a collimator limits the number of counts that are collected, thus decreasing detector efficiency and reducing sensitivity.[17] Nevertheless, imaging probes present two major advantages over counting probes: (i) allow for more precise detection of tumoral cells than acoustic counting probes, specifically when the area under investigation is near organs that might accumulate radioactive compound (i.e., the bladder); and (ii) images are helpful in evaluating complete resection.

2.1 | Basic components of nuclear probes

The physical principle upon which, both counting and imaging, nuclear probes rely is the detection of radiation to provide a measurable auditive or visual response, respectively, proportional to the total radiation being detected.[18] Two main detector categories are differentiated based on the materials used to stop the incoming radiation:

1. Ionization: These detectors are based on semiconductor materials that directly convert the incoming radiation into energy (direct conversion). As shown in Figure 3, when a γ-ray traverses, the depletion layer generates the movement of electrons and holes, which produces an output signal proportional to the number charges conducted. Semiconductor detectors provide good energy performance and enable the rejection of scattered events (i.e., Compton interactions). However, semiconductor detectors are disturbed by temperature changes, charge polarization, and require complex electronic circuits.[19] Yet, the introduction of application-specific integrated circuits (ASICs) has partially alleviated the readout complexity. Typical semiconductor materials are cadmium–zinc–telluride (CdZnTe, also known as CZT) and cadmium telluride (CdTe). The high counting efficiencies of semiconductor detectors for beta and lower energy

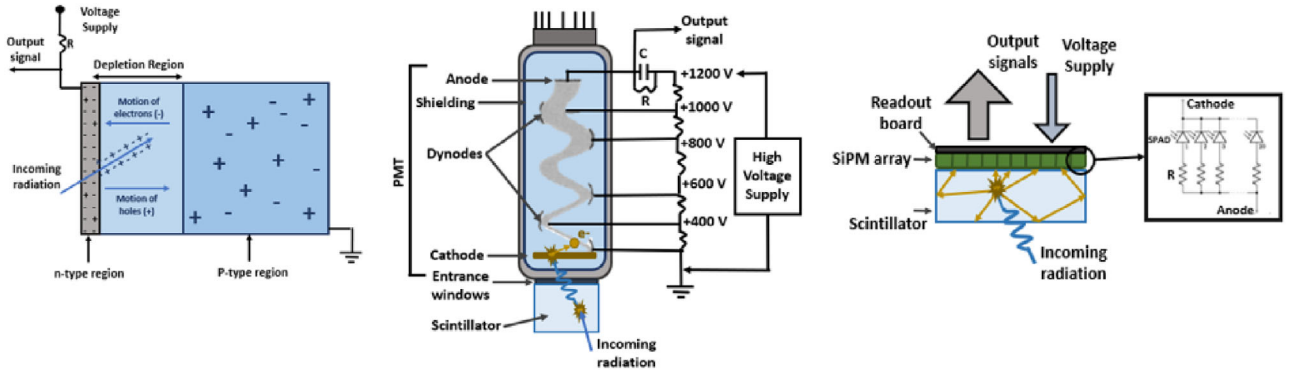

FIGURE 3 Left, schematic of a semiconductor detector; center, schematic of a scintillation detector coupled to a PMT and two scintillation detectors; and right, schematic of a scintillation detector coupled to an SiPM. PMT, photomultiplier tube; SiPM, silicon photomultiplier

gamma make them suitable as intraoperative beta probes.[20]

2. Scintillator: These types of detectors require the arrangement of a scintillation material and a photodetector to generate readable signals. Scintillator materials possess a higher density and Z_{eff} than semiconductors, thus providing a greater likelihood of photoelectric interactions. Current scintillators manufacturing techniques can fabricate consistent crystals of a variety of dimensions that, combined with recent developments in photodetector technology, made scintillator-based detectors a very attractive solution.[21] Scintillation materials can be divided into two groups:
   a. Organic scintillators: These are characterized by a fast response, thus being preferred for timing measurements and fast neutron detection. However, they generally present low light yield and their radiation length is tens of cm, thus leading to reduced sensitivity for energetic gamma particles and larger probabilities of Compton scattering interactions.
   b. Inorganic scintillators: These exhibit higher light yield and linearity of response than organic materials, which results in better energy performance, but their temporal response is slower. Because of their high density and small radiation length (~1–3 cm), they are appropriate for spectroscopy measurements and radiation detection.[22] Common inorganic scintillators are BGO, LYSO, or CsI(Tl), among others.

Both ionization and scintillation detectors have been commercially implemented in γ-ray detectors.[20] During the last years, the scintillation configuration has gained more interest, being the common probe structure based on a scintillator (to stop the incoming radiation) coupled to a photodetector (to convert the detected radiation into measurable signals), and an electronic readout chain (to produce visual, auditory, or both signals).

Regarding the photodetector, most of the nuclear probes currently available or under investigation employ photodetectors based on vacuum technology (Figure 3 center) such as photomultiplier tubes (PMTs) and multichannel PMTs (MC-PMTs), or based on semiconductor technology (Figure 3 right) such as photodiodes (PIN), avalanche photodiodes and silicon photomultipliers (SiPMs). Semiconductor detectors offer several advantages over the vacuum ones, such as insensitivity to magnetic fields (allowing their use within a magnetic resonance imaging system), a larger market of suppliers, and can be manufactured in a compact format with different customizable geometries. Indeed, solid-state-based nuclear probes have already demonstrated excellent performance.[23] Table 2 reports the most relevant properties of the photodetectors used in nuclear probes.

2.2 | Performance parameters of nuclear probes

The main parameters of interest to evaluate when ensuring the probe´s (counting or imaging) optimal performance depend on the design and components chosen for its assembly. Usually, a nuclear probe's evaluation considers the following quantities:

1. Energy resolution: It defines the probe's ability to discriminate different energies of the measured radiation thus reflects the ability to differentiate the activity coming from the lesion (i.e., tumoral target) from that of coming from other healthy parts of the body (background activity). The energy resolution is usually estimated as the ratio between the photopeak (E_{ph}) full-width-at-half-maximum and the centroid of the measured energy spectra.[24] For data acquisition, an energy window is usually defined, and only events with measured energy values falling in that range are accepted. Note that the width of the energy window depends on the probe energy resolution and impacts

TABLE 2 Main characteristics of the photodetectors encountered in nuclear probes

		Vacuum detector		Semiconductor detector		
		PMT	**MC-PMT**	**PN, PIN**	**APD**	**SiPM**
Detection efficiency	Blue (%)	30	20	60	50	40
	Green-yellow (%)	40	40	80–90	60–70	25
	Red (%)	<6	<6	90–100	80	10
Temporal resolution		100 ps	10 ps	1–10 ns	1–10 ns	1–100 ps
Gain		10	10–10	1	200	10
MRI compatibility		<10 T	Axial field 2 T	Insensitive	Insensitive	Insensitive
Mechanical properties		Delicate, bulky	Compact	Compact and robust		

Abbreviations: APD, avalanche photodiode; MC-PMT, multichannel photomultiplier tube; SiPM, silicon photomultiplier.

its performance by defining the portion of detected events that are accepted. Usually an energy window of $E_{ph} \pm 10\%$ is selected.

2. Spatial and angular resolution: These quantities only apply to imaging devices. The spatial resolution reflects the detector's capability to position incoming radiation and is defined as a measure of the smallest distance between two objects that can be resolved.[25] Including a collimator element is key achieving good spatial resolution but implies a reduction in sensitivity; thus, a tradeoff between spatial resolution and sensitivity has to be carefully studied. The angular resolution is expressed as the double value of the half opening of the detector's acceptance angle and it is affected by the distance and the fluctuation of scattered events being detected.[26]
3. Sensitivity: It relates to the probe's efficiency in converting the incoming radiation into a useable signal.[27] It is usually calculated as the number of detected counts as a function of the source activity and constitutes one of the most important criteria for the selection of a probe. There are two distinct components defining the sensitivity:
   a. Geometric sensitivity: It is defined as the fraction of emitted radiation that reaches the detector. Larger sensitive detector areas lead to higher geometric sensitivity and, for imaging devices, this quantity is inversely proportional to the collimator thickness.
   b. Intrinsic sensitivity (i.e., efficiency): It represents the fraction of radiation that is efficiently detected after impinging in the sensitive area of the detector. This quantity is proportional to the density, dimensions, and atomic number of the detector element.

Note that sensitivity is affected by the selected energy windows being larger for wider energy ranges, characteristics of the acquisition, and the attenuation of the radiation in the patient.[28] Thus, sensitivity is affected by tissue attenuation and decreases with depth following the inverse square distance law. Higher sensitivity has been reported for probes based on scintillation crystals; however, their accuracy is limited for profound lesions.

4. Contrast: It defines the probe's ability to distinguish activity in a specific area (i.e., tumoral area or SLN) embedded in a lower activity background region. It is usually calculated as the difference of the count rate measured for the target volume (N_T) and the background (N_B) as $(N_T - N_B)/N_T$). Contrast is affected by the detector sensitivity, spatial resolution (in the case of imaging probes), and energy performance.[24]
5. Count rate capability: It represents the maximum number of counts that can be detected before the detector saturates. For quantification purposes, it is of major relevance working in the linear response region of the detector, thus knowing the rate value at which the detector stops producing proportional responses to the amount of activity.[26]
6. Lateral and back shielding: These parameters are used to estimate how efficient are the collimators in blocking or reducing the amount of radiation reaching the detector that comes from emission sources in the surrounding of the target area. Note that side shielding helps to improve spatial resolution but at the cost of reducing the probe's FOV.
7. Geometrical design and scintillator dimension: The distance between the detector entrance face and the area being examined affects all the previously described parameters. On the one hand, smaller detector–tissue distances provide maximum sensitivity but low spatial and angular resolution. On the other hand, larger distances impose lower sensitivity at contact but enlarge the FOV, thus decreasing sensitivity dependence with depth. Therefore, a tradeoff between the device spatial resolution and global sensitivity should be considered based on the probe's application.

To accurately evaluate and compare the performance of different counting and imaging probes, two protocols have been outlined, namely, IT (Italian)[29] and NEMA

(National Electrical Manufacturers Association)[30] protocols.

2.3 | Types of nuclear probes

Nuclear probes are classified in different classes depending on the type of radiation to be detected namely, γ-rays, positrons (e^+), electrons (e^-), and Cherenkov photons (Ch).

2.3.1 | Gamma (γ)-probes

The first nuclear probe that was used intraoperatively (i.e., during surgical intervention) was employed to delineate brain tumors and was a γ-probe. Since its first appearance, the field of application of γ-probes (called γ-cameras when imaging is provided) has exponentially increased, and many producers already offer intraoperative γ-probes for radioguided surgery (RGS). The major field of application of γ-probes has been SLN detection and biopsy guidance. In 1997, Soluri et al. patented the first handheld γ-probe that is able to achieve high resolution. This device was used for detecting sentinel nodes and was constructed by coupling a CsI(Tl) scintillator to an MC-PMT array.[31,32] After some corrections to the initial design Soluri et al. performed the first imaging probe-guided biopsy in a breast cancer patient.[33]

Since then, most developed γ-probes were counting probes based on scintillation crystals coupled to photodiodes[34] or to semiconductor detectors such as SiPMs. Key parameter to consider when designing γ-counting probes, and counting probes in general, is their count rate capability and contrast. As high rates are expected closer to the lesion, tests using high-activity sources in different background conditions are performed when selecting the photosensor.

The main limitation of γ-counting probes is their inability to determine where the radiation is coming from, thus being sensitive to the nonspecific uptake of the radiotracer. This hardens the detection of small lesions, especially of tumors that are in the proximity of the radiotracer injection point or to areas in which the activity ratio of the tracer uptake in the tumor and surrounding area is small. To alleviate this limitation in positioning, lateral and back shielding, usually made of tungsten pieces, are used for blocking γ-rays coming from the surroundings areas of the lesion. Furthermore, the probe's detection efficiency is strongly impacted by the relative angular position and relative distance between the probe and the explored area that in turn will affect the geometrical efficiency of the probe (small probe–lesion distances imply maximum sensitivity but at the cost of lower spatial resolution).

The construction of high-performance γ-imaging tools (i.e., probes) allows us to overcome these limitations as they provide a 2D image of the radiotracer distribution in the body. In this way, it is possible to discriminate the tumor signal from the background, thus improving the device signal-to-noise ratio (SNR) that is necessary for RGS.

In this regard, the γ-camera geometrical efficiency benefits from short distances between the detector entrance face and the lesion as well as from intraoperative small FOV. Lateral shielding and back shielding are implemented to provide adequate FOV size as well as reducing the contribution of low-energy γ-rays in the image, which in turn enables better image contrast. However, one of the main problems associated with very small FOV (<4 cm^2) is the need to acquire multiple images to efficiently evaluate the surgical area and the difficulty in holding the probe for several minutes until the acquisition is completed. To mitigate this limitation, as can be seen in Table 3, larger FOV (>5 cm^2) γ-cameras have been developed and, to ensure stable positioning, mechanical parts are used. Figure 4 shows pictures of some of these probes.

Regarding the evolution of γ-cameras, it was in the 2000s when the first clinical trial using a γ-camera was presented by Scopinaro et al. The evaluation demonstrated a reduction of the SLN biopsy time because of the use of the probe.[37] Later in 2001, γ-cameras, based on semiconductor crystals (ZnCdTe), started to be developed but, due to the big scintillators and collimators, were too heavy to be used intraoperatively and usually required mechanical support to be moved. To overcome these handling limitations, Soluri et al. patented a novel probe design in which the scintillation crystals were introduced inside the collimator holes. This design exhibited better resolution and sensitivity than conventional designs allowing RGS and biopsy even for research in the preclinical field (i.e., with small animals). In 2002, Pitre et al. proposed the replacement of the multi-crystal array by a continuous planar crystal (monolithic technology[38]) coupled to a PSPMT[39] boosting sensitivity.

More recently, it has been proposed by using γ-cameras aided by laser beam pointers. The probe-laser beam approach has been already used intraoperatively for radioguided occult lesion localization (ROLL) and SLN biopsy improving surgical precision.[40] This technique has been also extended to the location of other malignancies such as small renal tumors.[41,42]

2.3.2 | Beta (β)-probes

There are clinical cases in which RGS based on γ-radiation detection is not possible due to the presence of uptaking organs nearby the area under investigation, such as in the brain or abdominal areas among others.[43] In this context, β-probes may constitute an excellent alternative as beta radiation (electrons and positrons)

TABLE 3 Examples of commercial γ-probes and γ-cameras, extracted from Refs. [35, 36]

	γ-Modality	Detector	ΦFOV (mm)	Spatial resolution (mm)	Energy range (keV)	Energy resolution (%)	Sensitivity (cps/MBq)	Manufacturer
C-Trak Automatic	Counting	CdZnTe	11	18 at 1 cm	27–364	21	2800	Care Wise (US)
Europrobe CsI	Counting	CsI	16	21 at 1 cm	110–1000	29	4500	Eurorad (France)
Europrobe CdTe	Counting	CdTe	11	15 at 1 cm	20–364	12	3200	Eurorad (France)
GammasonicsTM	Counting	CsI(Tl) + PSPMT	–	35 at 1 cm	27–200	38	1338	Inst. Medical Research (Australia)
Scinti-Probe MR100	Counting	CsI(Tl) + PSPMT	15	5 at 2 mm	30–385	24	380	Pol.Hi.Tech (Italy)
Scinti-Probe MR200	Counting	BGO + PSPMT	15	7 at 2 mm	30–600	35	220	Pol.Hi.Tech (Italy)
GammaFinder	Counting	CsI(Tl) + APD	10	20 at 1 cm	110–1000	10	11800	World of Medicine (Germany)
Neoprobe 2000	Counting	CdZnTe	14	15 at 1 cm	27–364	7	3070	Neoprobe Corp (US)
Navigator GPS	Counting	CdTe	14	13	37–364	–	21	United States Surgical Corporation
Wprobe	Counting	CsI + SiPM	11	8.65 at 1 cm	85–200	9	45000	Oncovision (Spain)
CarolIRes	Counting	YAP:Ce	10	8.5–13.7	27–364	56	13500	IPHC (China)
CXS-OP-SZ	Counting	CsI + PIN	15	17 at 1 cm	140–522	16	20000	Crystal Photonics (Germany)
High-energy PET probe	Counting	NaI	12	8	511	–	39000	Univ. of Lübeck (Germany)
TReCam	Imaging	PH + LaBr:Ce + MAPMT	50 × 50	0.9 contact	^{99m}Tc	11.3	300	–
Ez-Scope	Imaging	PH or PIN + CZT	32 × 32	2.0 at 1 cm	71–364	8.6	184	Anzai (Japan)
Minicam II	Imaging	PH+ CdTe	40 × 40	2.46	30–200	5–7	200 at 1 cm	Eurorad
Sentinella 102	Imaging	PH + CsI(Na) + PSPMT	40 × 40	5.7–8.2 at 3 cm	71–364	15.9	90–900 at 1 cm	Oncovision (Spain)
Intraoperative γ-camera	Imaging	PH + CZT	40 × 40	5 at 5 cm	40–200	8	100 at 5 cm	GE Healthcare (USA)
SSGC clinical type	Imaging	PH + CdTe	44.8 × 44.8	1.6 contact	550 max	6.9	150	Tsuchimochi (Japan)
IP Gardian II	Imaging	PH + CsI + PSPMT	49 × 49	2.2 intrinsic	^{99m}Tc	20	210	Li-Tech (China)
NodeView	Imaging	NaI(Tl) + PSPMT	50 × 50	1.8 at 0.6 cm	–	12	270	IMI (USA)

Abbreviations: APD, avalanche photodiode; FOV, field of view; PH, parallel hole collimators; PIN, pinhole; SiPM, silicon photomultiplier.

FIGURE 4 Examples of some commercial γ-probes and γ-cameras. (a) GammaFinder, (b) NeoProbe 2000, (c) Wprobe, (d) MiniCam II, (e) Sentinella 102

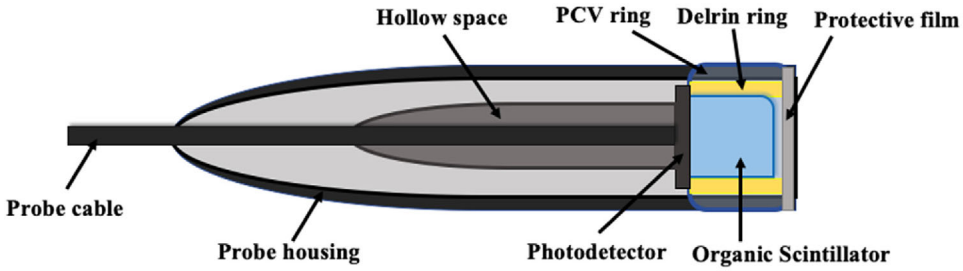

FIGURE 5 Basic configuration of a β-probe

has a short range in tissues (~1 mm), thus allowing for the detection of superficial radiation.

β-Probes are sensitive to a short range of radiation, thus avoiding the problem of background γ-radiation without the need for lateral and back shielding, while being more sensitive and accurate in localizing the tumoral lesions than γ-probes.[44] As in the case of γ-counting probes, special attention should be paid to the β-probes count rate capability as high rates are expected especially when detecting superficial radiation.

Nevertheless, as β-probes have to be in contact with the tissues under examination to provide high geometrical efficiency, their design suggests some technological constraints such as being compact, lightweight (<250 g), and easy to handle. Moreover, β-probes sensitivity has to be high enough to enable a fast detection (range of seconds to be time compatible with the surgical practice) of areas with low radiotracer uptake.

Regarding β-probe's spatial resolution, the quantity has to be in the order of just a few millimeters to improve the tumor SNR and must reduce the influence of the signal coming from the surrounding areas, thus also improving the tumor-to-background ratio, image contrast, and boosting detection efficiency. To account for this all, typical β-probe designs present diameter sizes between 8 and 15 mm with an active detector area of ~15–25 mm^2.[36] The external face of the probe is typically covered to protect the detector-sensitive area from external light. Conventional β-probes were based on plastic scintillation detectors,[45] but due to recent improvements in the photodetector technology, most of the existing β-probes or under development include semiconductor technology, see Figure 5 for a schematic of an SiPM-based β-probe.

Depending on the type of β particle detected, β-probes are grouped into two main categories, namely, positron (β^+) or electron (β^-) probes, and their selection depends on the target application, as described in the following.

Positron probe (β^+-probe)

Positrons (β^+) are direct ionizing particles, meaning that the deposit of its energy occurs via elastic scattering from nuclei or inelastic collision with other electrons encountered in the medium (i.e., tissue). Note that, due to the energy typically encountered in clinical applications (few MeV or less), only a small portion of the energy loss is caused by direct radiation emission.

The positrons detected with the probes are produced inside the patient body as the decay product of a radiotracer that is usually injected to perform Positron Emission Tomography (PET) imaging. These emitted positrons travel a short path inside the patient body before annihilating with an electron in the tissue; thus deep emitted β^+ annihilates before reaching the detector.

β^+-Probes aim therefore for the identification of superficial radiation and usually include metallic shielding or protective films at the entrance face of the detector to block incoming electrons. Intraoperative β^+-probes based on semiconductor technology have demonstrated to perform best for lesion localization and postoperative control of the excision cavity,[46] and its performance depends on the scintillator material, light window, shielding, optical reflectors, and photosensor technology.

Several studies have been performed, both based on simulations and experiments to determine the best β^+-probe design. In these studies, special attention was given to the study of the optimal probe's energy range for operation as it directly impacts sensitivity. In Ref. [35], for example, the authors evaluated, through Monte Carlo simulations, different β^+-probe designs based on a scintillator, including optical reflectors and then coupled to an array of SiPMs including a spread window in between. The design provided an FOV of 25.7×25.7 mm^2 and the readout comprised two ASICs. Another example is the probe scheme presented in Ref. [47] in which the probe was united with a biopsy or excision tool for the simultaneous detection and removal of the target tissue.

Other studies have already demonstrated that β^+-probes are feasible to detect tumors of ~2 mm in diameter,[48] guide breast tumor excision[49] and exploration of known or suspected metastatic diseases.[50] Table 4 reports the main characteristics of some developed counting and imaging β^+-probes, and this information is extracted from Ref. [36] and references therein.

Electron probe (β^--probe)

Pure β^- particles are able to penetrate only a few millimeters in tissues without generating almost no γ-radiation, thus resulting in a high tumor-to-background ratio and providing a clearer delineation of the tumoral margins.[51]

The design of β^--probes follows a similar approach to the one used in β^+-probes.[52] Different configurations have been proposed and investigated for the development of β^--probes.[53] Usually, these designs are based on using nonhygroscopic, low density, and high light yield scintillators such as *para*-terphenyl. In Ref. [54], for example, the authors investigated a radiation-sensitive scintillator tip made of commercial *para*-terphenyl showing good performance.

β^--Probes are very compact, achieve good sensitivity to electrons, are almost transparent to bremsstrahlung radiation, yield to millimetric spatial resolution, and provide a fast response. In most β^--probes design, the detector head is assembled on top of a cylindrical body of a 7–10-mm diameter and 14-cm length (depending on the application), and the generated scintillation light is conducted using optical fibers till the photodetector that is placed outside the probe's holder. However, it should be pointed out that, β^--probes are less interesting from a medical point of view than β^+-probes due to a more reduced selection of radiotracers available.

2.3.3 | Dual probes: beta and gamma (β/γ-probes)

To take advantage of both modalities' features, the development of hybrid dual probes (β/γ-probes) has been proposed. These dual probes usually include two detectors: one for positrons detection and the other one for gamma-radiation detection.[55] Dual probes are of particular interest for intraoperative F-fluorodeoxyglucose (FDG) localization as the γ-sensitive probe is used to identify tumors, whereas the β-sensitive one is employed for assessing PSM.[33]

The operation principle of dual probes is based on detecting both the positron and gamma particles coming from the patient using two different detectors combined in one unique detector head. The number of detected counts in the second detector (usually the gamma detector) is subtracted from the number of counts collected in the first detector (positron sensitive one), thus providing an estimation of the number of detected positrons that is an indicator of the presence of radiotracer compound within few millimeters from the surface. It should be noted that the detectors building the dual probe do not present the same efficiency in detecting gamma particles, which implies that before subtracting the number of counts from the first detector, the recorded events of the second one should be corrected by applying a weighting factor considering the variance in efficiency for such particles.

Raylman et al. developed a dual β/γ-probes which consisted of two solid-state detectors that could be operated in two modes,[56] namely, β- and γ-optimized modes. In their detector design, the difference between the signals coming from the β- and γ-optimized detectors was used to subtract the gamma contribution to the signal coming from the β-optimized detector. The most relevant finding of this work is the reported gamma-detection sensitivity, which suggested that the dual design may enable the implementation of dual-radiopharmaceutical procedures.

In the following years, other dual probe designs were proposed and evaluated reporting good performance. Due to the interest and excellent performance shown in this hybrid approach, commercial designs such as the dual probe are manufactured by IntraMedical Imaging (Los Angeles, CA, USA).[57]

2.3.4 | Cherenkov luminescence probes: (CL-probes)

Cherenkov luminescence probes (CL-probes) are based on the optical molecular modality of Cherenkov luminescence imaging (CLI),[58] which relies on the detection of the Cherenkov yield produced in tissues.

Note that, after injecting the radiotracer, PET systems measure the γ-rays resulting from the positron–electron annihilation, whereas CLI measures the Cherenkov photons generated by these charged particles (e^+ or e^-) while traveling at faster speed than the speed of light through the tissue.[59] Note that, while in PET imaging the achievable spatial resolution is limited by the range of the positron, in the case of CLI, as the positron path

TABLE 4 Characteristics of some developed counting and imaging β^+ probes, extracted from Ref. [36] and references therein

	β-Probe modality	Detector	FOV (mm)/Det. area (cm^2)	Spatial resolution (mm)	Sensitivity (cps/kBq)	γ-Noise rejection
Yamamoto et al.	Counting	BGO +Platic. Scint + PMT	8	11 at 5 mm	2.6 at 5 mm	Coincidence
Raylman et al.	Counting	Si	16.5	3 at 0.5 mm	195 at 1 mm	Substraction
β-Probe (Intra medical)	Counting	PMT + Platic. Scint	5.5	10 contact	108 at contact	Substraction
β-Probe (Silicon Instrumental)	Counting	Si	16	8 at 1 mm	243 at 1 mm	–
CSX-OP-β	Counting	PIN	12	8 at 6 mm	20 contact	–
Camillocci et al.	Counting	p-terphenyl + PMT	5	2.8 at 0.4 mm	–	–
Yamamoto et al.	Imaging	CaF_2:Eu + PSPMT	3.1–12.5	–		Coincidence
Gamelin et al.	Imaging	Scint fiber + PMT	0.27	–	3 at 1.5 mm	–
Levin et al.	Imaging	CaF_2:Eu + BGO + PMT	1.2	0.5	230 contact	–
Liu et al.	Imaging	Plastic Scint+ GSO + MC-PMT	2.5	2.0	78–194 contact	Coincidence
Stolin et al.	Imaging	Plastic Sinct. + SiPM	1.7	2.5	108 contact	–
Russo et al.	Imaging	Silicon + Medipix2	1.98	0.23 contact	317	–
Tipnis et al.	Imaging	CSI:Tl + CCD	25	–	216 contact	–
Sabet et al.	Imaging	CsI:Tl + LYSO:Ce + SiPM	1.3	0.8	–	Substraction
Bogalhas et al.	Imaging	Plastic Scint+ GSO:Ce + PSMPT	2.3–5	1.6	217	Substraction
Visvikis et al.	Imaging	CCD	0.98–2.4	0.132–0.176	75	–
Hudin et al.	Imaging	Plastic Scint. + GSO:Ce + SiPM	1.6	0.5	340 contact	Substraction

Abbreviations: CCD, charge-coupled devices; FOV, field of view; MC-PMT, multichannel photomultiplier tube; SiPM, silicon photomultiplier.

TABLE 5 Characteristics of common radionuclides that generates CL

Isotope (Decay particle)	Half-life ($t_{1/2}$)	Endpoint energy (keV)	Fraction above C_{th} (%) in tissue ($n = 1.4$)
^{18}F (β^+)	109.8 min	633	58
^{90}Y (β^-)	64.1 h	2280	93
^{131}I (β^-)	8.02 days	606	37

Abbreviation: CL, Cherenkov luminescence.

before generating Cherenkov radiation is smaller than the positron range, the spatial resolution is expected to be better. Moreover, the wavelength of Cherenkov photons is predominantly in the ultraviolet (UV) and blue areas of the electromagnetic spectra. In this region of the electromagnetic spectra, photons are attenuated by biologic tissue; thus, CLI is restricted to the detection of very superficial radiation (<3 mm from the surface in tissue),[60] and lateral and back shielding are used to block high-energy γ-rays coming from the surrounding tissues. Table 5 summarizes information for a few common radionuclides used in PET or SPECT that also generate CL.

Independently of the radioisotope energy, the emission of Cherenkov radiation is produced close to the radionuclide position (within a few millimeters) and can be produced in biological tissues directly by the primary β particles: (1) passing through the tissue, or by secondary electrons with kinetic energy beyond the Cherenkov threshold. These electrons can be delta (δ) rays produced by the primary charged particles (2), Compton- of photo-electrons produced by the emitted γ-ray (3). The Cherenkov emission can result also from Bremsstrahlung radiation (4). See Figure 6 (left part) for an explanatory drawing of these processes.

Because of the optical properties of tissues, CLI requires using high sensitivity charge-coupled devices (CCD) combined with optical lens and light-shielded housings,[62] Figure 6 (right part) shows a conceptual scheme of a CCD-based probe. Commercial devices that have been already used for CLI detection are the detector from the IVIS series[63]: intensified CCD and electron multiplying CCDs cameras,[64] or PMTs coupled to fiber optics and SiPMs.[61] Figure 7 summarizes the type of radiation encountered when injecting a radiotracer in the patient and the type of detector suitable for each one. In addition, CCD-based detectors have already demonstrated good performance at high rates; thus, they are ideal candidates for detecting high-activity lesions.[65]

CLI provides a favorable tool to detect superficial β-radioisotopes.[66] The use of CL-probes for dosimetry validation in radiotherapy and proton therapy, monitoring in vivo dosimetry, laparoscopy and endoscopy,[67] and RGS has already been reported.[68,69] Furthermore, CL-probes have been successfully used intraoperatively for tumor delineation and resection, as well as to determine PSM. It is worth noting that CLI can be performed without administering any additional radiotracers, to the ones injected for the presurgery SPECT or PET scan.

Recently, research groups have been investigating CL-probes and their applications. In Ref. [70], for example, the authors used CL-probes to show the correlation between total ^{18}F-FDG uptake for detecting tumors, and in Ref. [71], the authors reported the use of an intraoperative CL-probe to detect PSM after prostatectomy showing that tumoral cells were effectively detected. Similarly, in Ref. [72], the authors used a Cherenkov probe to detect PMS in breast cancer patients. Note that the CL-probes used in these studies were not optimized for intraoperative imaging, and the detections of cancerous cells were performed in vitro after excising the specimen (prostate or breast); thus, a handful, small, intraoperative CL-probe is still lacking.

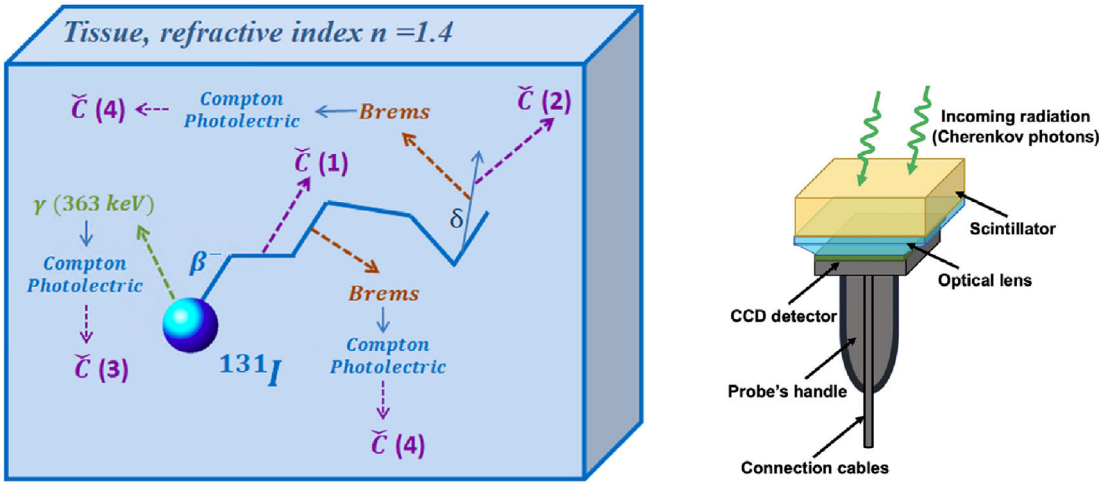

FIGURE 6 Left, schematics of the processes responsible for Cherenkov radiation emission, adapted from Ref. [61]. Right, conceptual scheme of a CCD-based probe. CCD, charge-coupled devices

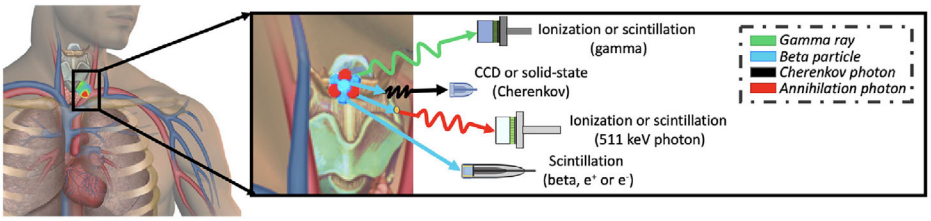

FIGURE 7 Schematics of the different types of radiation encountered when injecting a radiotracer in the patient and the most suitable detector for each one

2.4 | Alternative to nuclear-probes: fluorescent probes (FL-probes)

Despite the numerous advantages provided using nuclear probes, they rely on exposure to radiation during intraoperative assessment. To avoid this, probes based on other modalities such as near-infrared fluorescent probes (FL-probes) are being investigated.[73]

Fluorescence is a physical process in which light of a specific wavelength, usually 300–800 nm, is emitted due to the returning of an excited electron to its equilibrium state. FL-imaging constitutes a noninvasive imaging technique and is commonly used for biochemical applications such as the visualization of biological processes in living organisms.[74]

However, the use of FL-imaging is limited by the photobleaching phenomenon that damages the molecules and reduces its fluorescent.[75] Moreover, the efficiency of FL-probes is extremely affected by several factors such as nonuniform tissue illumination, temperature changes, or absorbers that reduce or even block the fluorescence signal.

Recently, label-free fluorescence lifetime imaging (FLIm) has been proposed for guiding medical interventions since uses tissue autofluorescence thus avoiding the injection of any other contrast or chemical agents.[76] By exploiting FLIm techniques, the limitations previously mentioned for conventional FL-imaging may be overcome.

3 | THE "IDEAL" PROBE, DESIGN CONSIDERATIONS

When selecting a medical tool, several factors should be carefully considered such as performance of the most relevant physical parameters, namely, spatial resolution, FOV size (in the case of imaging devices), energy resolution, detection accuracy (i.e., sensitivity), and temporal performance. Moreover, hardware features such as the display screens or quality of the auditive signal are also important as this affects the probe's ergonomics, the quality of the service, and cost.

In the case of nuclear probes, it should also be evaluated the ability to distinguish the lesion from the injection point and background radiation; thus, sensitivity and contrast are also important.

In principle, as different instrumentation technology is used for different types of probes and applications, an ideal probe would be built using available technology, with good specifications, in all types of possible emissions, namely, beta (both β^+ and β^-), gamma (γ) either from annihilation or from scintigraphic radiotracers, and Cherenkov (Ch).[77,78] As gammas have a longer absorption length than β or Ch, the background can be difficult to isolate; hence this mode of operation is perhaps the least appealing.

If we look to β- and Ch-based probes, we realize that both modalities have sub-centimeter absorption lengths, rendering them ideal for positivity margin detection. Given that in some presurgery protocols, radiotracer administration is foreseen within 24 h before surgery, and that common radiotracer half-life is comparable to that, it is safe to assume that existing protocols have considered the safety of the patient and clinical personnel in particular concerning their radiation exposure. Hence, an ideal new probe technology will not require a significant expansion of existing protocols but will be able to detect existing pre-administered radiation. Particularly for protocols using PET imaging radiotracers, both β^+ and Ch radiations are delivered. Hence, we focus on the detection of these two particles.

The ideal detector should have, therefore, good discrimination between the different particles, supported by strong background noise rejection. A good energy resolution would help this. It should also present a linear response for high counting rates, thus allowing for a simple counting function to the extent that this is required by the medical professional, coming from low dead time, but also be able to provide quality imaging, through sufficient spatial resolution. In this regard, the selection and enhancement of the photosensor technology are key. Recent solid-state silicon-based detectors provided significant spatial resolution and broad particle detection capabilities. Considering the example of Medipix4, a silicon tile built for high-energy physics experiments at CERN,[79] UV photons, and β particles are clearly distinguishable on their detection signatures. This means that a probe based on such technology not only has multimodal capabilities but is also able to provide accurate simultaneous multimodal

measurements, allowing readout signal analysis to provide readily and real-time information on the relative presence of particles, leading to optimal localization of lesions within millimeters from the probe.

On top of detecting capabilities, it would be ideal to design specific chips that include its associated readout, firmware, and software for data processing, thus allowing for quick prototyping, development, and commercial manufacturing. The type of chips required could be connected or loaded in custom hardware like microprocessors or an FPGA such as the *Zynq* of *Xilinx* allowing both programmable logic and good quality microprocessing. As such, a probe based on this technology can become a breakthrough for the field.

Similar technology is applied in transmission electron microscopy, which guarantees the functionality of the detector as a β-probe-applied tool, although weight is not directly evaluated. However, such detectors, using semiconductor technology such as Si, GaAs, and others, have strong spatial distribution and energy resolution, rendering them ideal for imaging configurations.

Novel nuclear probe designs aim to improve state-of-the-art (SOA) technology for both counting and imaging instruments that should be possible by including all previously mentioned considerations. Regarding gamma detection, commercial counting probes have already reported energy resolutions as good as 7% and sensitivity values of 3070 cps/MBq for an FOV of 14 mm in diameter (see Neoprobe 2000 in Table 3), whereas imaging γ-probes are able to provide spatial resolution values of 0.9 mm at contact and reported sensitivity values of 300 cps/MBq for a 50 $\times$ 50-mm^2 FOV (see TReCam in Table 3); however, the energy resolution attainable using this nuclear probe is just 11.3%. Thus, the tradeoff between energy and spatial resolution when designing the ideal probe has to be considered and will depend mostly on the probe's application. Such a tradeoff is obtained with an SSGC clinical camera from Tsuchimochi (Japan), which provides spatial and energy resolution values of 1.6 mm at contact and 6.9%, respectively, and a sensitivity of 150 cps/MBq for an FOV of 44.8 $\times$ 44.8 mm^2.

Regarding β-radiation, it has already been reported spatial resolution values as good as 0.5 mm for an FOV of 1.6 cm^2 using β-probes (see Hudin, et al., in Table 4), which includes a subtraction method to eliminate the γ contribution in the acquired data. The sensitivity of this probe is 340 cps/kBq at contact. Therefore, new imaging probe designs should target spatial resolutions $<$1 mm, while providing energy resolutions $<$7% in an FOV $>$ 50 mm^2 for the detection of γ, β, or Ch radiation. Moreover, the design should provide high sensitivity.

In addition to the abovementioned technological requirements for the design of the ideal probe, it has to be pointed out that, to provide useful outcomes, nuclear probes require extensive data processing and, in the case of imaging probes, accurate image reconstruction methodologies. Moreover, automated feature selection, segmentation, and classification techniques have to be applied to the reconstructed images to identify which patients would benefit from intervention or which type of treatment better suits the patient condition (i.e., tumor resection or radiotherapy, among others). Also, due to the absence of background anatomical information, the presence of residual noise, insufficient image quality, and weak signals, interpreting the images provided by imaging probes is not always easy and may lead to inaccurate and unreliable diagnoses as well as tedious and time-consuming patient staging.

In the recent years, the introduction of artificial intelligence (AI) algorithms, in particular neural network (NN) machine learning approaches, has shown promise to face the abovementioned challenges. Machine learning approaches have already been implemented in other nuclear imaging applications[80,81] to alleviate technological limitations such as noise reduction, signal identification, or data processing among others, as well as limitations during the image reconstruction process. Moreover, innovative NN methodologies have already proven to be useful tools in the management of large and complex data sets, image denoise,[82] and image segmentation.[83] Current machine learning approaches can be modified and combined with nuclear probes to overcome the abovementioned limitations, boost the probe application, and extend their clinical use. Thus, as described in the following section, innovative nuclear probes should be combined with novel and accurate machine learning algorithms.

3.1 | Machine learning and nuclear probes

In the case of nuclear counting probes, introducing machine learning algorithms may improve and fasten the calibration procedures of the probe and ensure a linear response at high counting rates. In this regard, NNs could be trained to identify the optimal signal level and then, remove saturated/noisy signals,[84] see Figure 8 for example. Similarly, the introduction of NNs might help improving the SNR of counting probes as this parameter is usually compromised by the presence of background radiation coming from surrounding tissues, especially when the presence of radiotracer in the area under study is low. To do so, the network topology could be trained to suppress noise and other related artifacts from the input signal, as, for example, in the approach presented in Ref. [85] in which the authors implemented a convolutional NN (CNN) for image noise reduction in low-dose computed tomography (CT) images. For the counting probe case, the network will receive as inputs the acoustic signals instead of images and would be trained to denoise and magnify the acoustic signals that

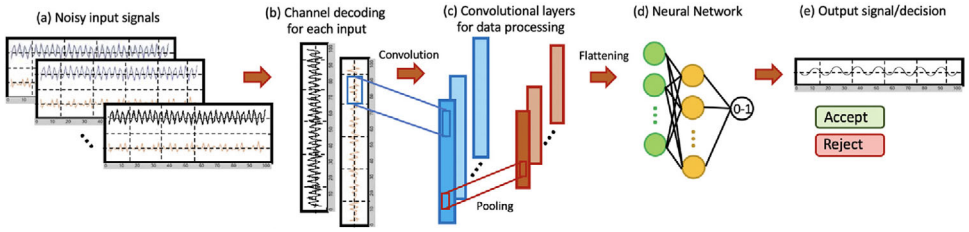

FIGURE 8 Exemplification of the application of a CNN for signal denoise in nuclear counting probes. CNN, convolutional neural network

come from the lesion while suppressing the ones coming from its surroundings.

Yet, it is with imaging nuclear probes, both γ- and β-probes, where machine learning approaches could be of major interest. In the imaging context, machine learning can be employed to reduce image noise, improve image contrast, and thus enhance diagnostic quality. Several approaches have been implemented for different imaging modalities during the last years, such as the constrained by the identical, residual, cycle learning ensemble, which resulted in a twofold resolution improvement for MR and CT images[86] and also allowed to retrieve high-resolution images from low CT resolution acquisitions.[87] Complementary to these SOA works, in Ref. [88], the authors included the Wasserstein distance–guided domain[89] to enforce the cycle-consistency and establish a nonlinear mapping from noisy low-resolution input images to noise-free high-resolution outputs. Following these methods, NNs and CNNs ensembles could be trained to learn the background noise patterns commonly observed when using γ- and β-imaging probes and to provide noise free images. Moreover, including AI during the image reconstruction might reduce artifacts and generate denoised images.

With the aim of improving image reconstruction and ease the learning process of anatomical features, in Ref. [90], the authors proposed a contrastive voxel-wise representation learning in CT images and, in Ref. [91], presented and validated an improved methodology named simple contrastive voxel-wise representation distillation (SimCVD) for CT image segmentation, which significantly improved SOA voxel-wise representation learning.

Also, machine learning can be employed to quantify the total tumor volume, the extension of the resection area, the presence of PSM (i.e., the main areas in which nuclear probes are employed), and the correlation of image features with clinical endpoints.[81] Studies have already reported the improvements obtained when using CNN for tumor margin classification in head-and-neck cancer,[92] brain tumors[93] or breast malignancies,[94] among others.

Regarding FL-probes, machine learning procedures might help to overcome some of the limitations presented in Section 2.4. In Ref. [95], for example, the authors reported a nuclear segmentation tool (NuSeT) based on deep learning to accurately segments nuclei across multiple types of fluorescence imaging data. Similar approaches could be implemented in FL-probes to reduce false positives.

In conclusion, machine learning algorithms should be considered and implemented in the next generation of nuclear imaging probes.

4 | CLINICAL APPLICATIONS OF NUCLEAR PROBES

High performance medical probes, such as the ones described earlier, are relevant for multiple clinical applications and constitute key medical instruments in the control of different pathologies.

Since the first reported intraoperative tumor localization using a counting probe in 1951,[14] several efforts have been taken to enhance nuclear probe performance. It has been already proven the feasibility of using nuclear probes for tumor delineation using RGS intraoperative margin evaluation after injecting a radiotracer. β- and CL-probes have demonstrated superior performance than gamma probes for PSM and resection. Counting probes are preferred for this application because no image is needed as the probes are used to confirm the precise localization of a lesion that was previously identified.[79] Recently, it has been proposed by using counting probes as a complementary tool to other imaging modalities, as using fast counting probes, compared to the detection of γ-rays, improves real-time tumor localization.[96] In this context, radioguided protocols have been already outlined, such as ROLL.[40]

Regarding imaging nuclear probes, the enhanced sensitivity and spatial resolution when compared to SPECT or PET scanners enable a better detection of small lesions. γ-Cameras are the preferred type of imaging probe as they achieve excellent spatial resolution and high specificity for SLN identification. The enhanced sensitivity and spatial selectivity of SOA imaging probes combined with the absence of background noise (insertion of a collimator) allow one to decrease the dose injected to the patient and, thus, the one received by the clinical personnel.[97]

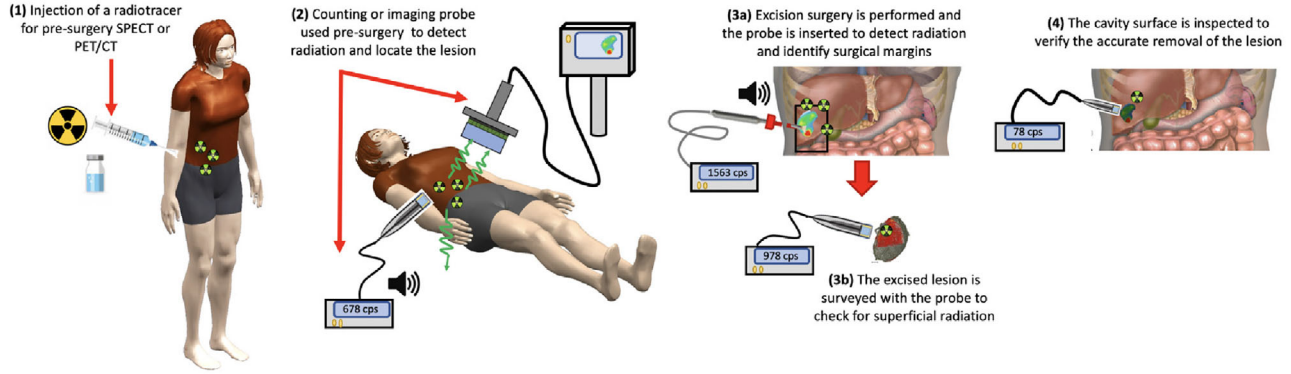

FIGURE 9 Exemplification of the clinical methodology usually followed: (1) radiotracer compounds are injected for presurgery SPECT or PET/CT imaging, (2) counting or imaging probes are used presurgery to detect the presence of radiation and locate the lesion, (3) resection/excision surgery is performed and the probe is inserted to determine surgical margins. The excised lesion is surveyed with the probe to check for superficial radiation, and (4) the resection cavity is inspected to confirm the precision of the surgery. CT, computed tomography

As in the case of β-probes, CL-probes are of special interest for the detection of superficial radiation and thus for an improved assessment of PSM. CLI is used in lymph nodes detection, endoscopy applications, and for the detection of superficial cancer such as gastrointestinal tract cancers that are cutaneous cancer.[98] Preliminary studies using CL-probes have shown promising results despite the fact that the sensitivity achieved by CL-probes is much lower than the one reached by probes based on scintillators coupled to photosensors.

Regarding applications, one of the main uses of both counting and imaging probes is to precisely guide surgery (i.e., RGS) by providing information for the localization of hidden or challenging access lesions such as tumors. Nuclear probes are also used for clinical assessment thus to perform less invasive surgery and have already been demonstrated to be fundamental in the clinical routine for SLN biopsy as well as in the guidance of tumor resection, PSM identification, and biopsy.[99]

High-efficiency probes could enhance patient prognosis by enabling more accurate identification of the SLN as this increases the probability of completely removing the surrounding metastatic areas.[100] Furthermore, the uses of nuclear probes (both counting and imaging) have also demonstrated promising results for the detection of other cancer types such as vulvar, cervical and breast cancer, melanoma and other cutaneous malignancies, oral cavity cancers, prostate, head and neck, and urological cancers in general.[101]

Nuclear probes are also used for noninvasive RGS. Figure 9 shows the mostly used methodology in RGS with nuclear probes. RGS methodology describes as follows: A radiotracer is injected (presurgery) into the patient for determining the exact tumor size and location via SPECT or PET/CT imaging; then an accurate nuclear probe (counting or imaging, depending on the type of malignancy) is used for an exact tumor location. The next step is to start the intervention, in which probes are used intraoperatively at this stage for a precise definition of tumor margins and the tumoral region is excised. Finally, the probe is used again to confirm that tumoral areas do not remain and to validate the efficacy of the surgery before patient closure. Postsurgery imaging may be used in some cases to confirm the accuracy of the resection.

Considering all previously mentioned advantages and applications of nuclear probes, using these devices may allow for an enhanced management of cancer as well as other metabolic diseases, for example, in the evaluation of prostate cancer (PCa) patients. PCa is one of the most common cancer deaths among men.[102] Regular procedures followed for PCa identification are to evaluate the level of prostate-specific membrane antigen in the blood followed by digital rectal inspections. After that, if PCa is suspected, transrectal biopsies of the prostate are carried out to confirm PCa.[103] However, biopsies sample random parts of the prostate, and therefore, it is possible to omit regions where cancer is present, thus leading to an incorrect diagnosis. In addition, biopsies are painful and often require hospitalization. Here, guiding biopsies using counting or imaging nuclear probe may be key to enhancing diagnoses.[101] Figure 10 provides a schematic of the procedure followed in PCa management comparing blinded biopsy and probe-guided biopsy.

Similar to PCa, it occurs with kidney cancer, liver cancers (which are one of the most fatal cancer types with incidence and mortality rates of 4.7% and 8.3%, respectively[1]) or to all cancer types that require resection or biopsy.[42] In general, the 5-year survival rate of cancer patients depends on several factors such as the stage of the disease, the tumoral spreading to surrounding tissues, organs, regional lymph nodes, or to other parts of the patient body.[104]

The survival rate and the prognosis of the patient could be improved by accurately locating PSM during tumoral resection or by guiding biopsy procedures. For example, in Ref. [105], the authors report the use

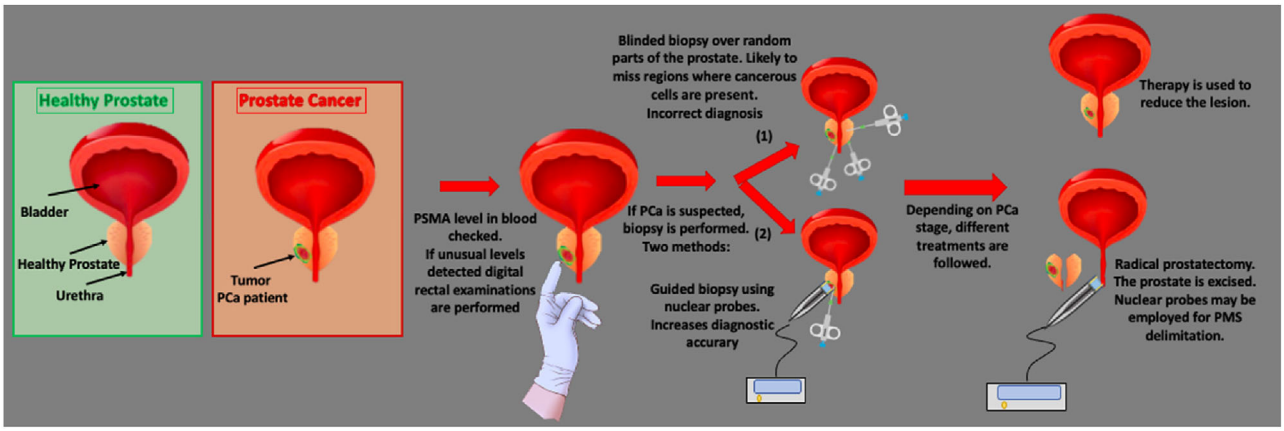

FIGURE 10 Exemplification of the clinical procedure followed in PCa management, including blinded biopsy and probe-guided biopsy. PCa, prostate cancer

of γ-imaging probes assisted by the ROLL technique for an enhanced location of small renal tumors; in Ref. [100], the other group reports the use for breast tumor identification; and in Ref. [101], for assessing radical prostatectomy—all of them reporting promising outcomes associated with the intraoperatively use of nuclear probes.

5 | CONCLUSION

Nuclear medicine and, in particular, molecular imaging have been demonstrated to be the area for helping developments toward noninvasive clinical applications such as patient malignancy staging, lesion identification (i.e., SLN, tumors or other malignancies), surgical management of lesions, RGS (i.e., PSM assessment and biopsy), treatment monitoring by checking the amount of radiation delivered in a certain area, or dose optimization among others.

Nuclear medicine probes have proven to be useful medical tools for the abovementioned applications as well as the precise location of other occult lesions.

In the present manuscript, a review highlighting the development, basic components, and current SOA nuclear medicine probes technology has been presented followed by a description of the types (i.e., counting and imaging) and key performance parameters of these probes, namely, global sensitivity, spatial resolution, and spectroscopy capabilities (i.e., energy resolution). This document also provides a brief explanation of the physics underlying each element building the probe's detector such as scintillators crystals and semiconductors, vacuum and solid-state photosensors, as well as the different types of probes based on the target radiation nature (i.e., gamma, beta, and Cherenkov). Finally, SOA probes are reported in the manuscript. After going through the present manuscript, the reader should be aware of the practical considerations in designing, selecting, and using intraoperative probes.

To summarize, nuclear probes are key components of molecular imaging; thus, research should continue investigating the "ideal probe" design, and efforts should be taken to develop novel imaging probes beyond SOA technology.

ACKNOWLEDGMENTS

This work was supported in part by the "Grants for coordinated projects UPV—La Fe 2021; subprogram of preparatory actions" (IIS-F-PG-22-02). Andrea Gonzalez-Montoro is supported by VALi+d Program for Researchers in the Postdoctoral Phase of the Ministry of Labor and Social Economy (Generalitat Valenciana) and the EU Social Fund.

CONFLICT OF INTEREST

The authors have no relevant conflicts of interest to disclose.

DATA AVAILABILITY STATEMENT

The data supporting the results of this study are available upon reasonable request to the corresponding author.

REFERENCES

1. Sung H, Ferlay J, Siegel RL, et al. Global cancer statistics 2020: GLOBOCAN estimates of incidence and mortality worldwide for 36 cancers in 185 countries. *ACS J*. 2020;71(3):209–249.
2. National Cancer Institute. "Cancer Statistics". U.S. Department of Health and Human Services, 1-800-4-CANCER, 2020; Available at: https://www.cancer.gov/about-cancer/understanding/statistics
3. Makuuchi M, Kosuge T, Takayama T, et al. Surgery for small liver cancers. *Semin Surg Oncol*. 1993;9(4):298-304.
4. Poon RTP. Optimal initial treatment for early hepatocellular carcinoma in patients with preserved liver function: transplantation or resection? *Ann Surg*. 2007;14:541-547.
5. Pawlik TM, Scoggins CR, Zorzi D, et al. Effect of surgical margin status on survival and site of recurrence after hepatic

resection for colorectal metastases. *Ann Surg*. 2005;241(5):715-724.
6. Scheele J, Stangl R, Altendorf-Hofmann A, Gall FP. Indicators of prognosis after hepatic resection for colorectal secondaries. *Surgery*. 1991;110(1):13-29.
7. Adam R, Kitano Y. Multidisciplinary approach of liver metastases from colorectal cancer. *AG Surg*. 2019;3(1):50-56.
8. Yossepowitch O, Briganti A, Eastham JA, et al. Positive surgical margins after radical prostatectomy: a systematic review and contemporary update. *Eur Urol*. 2014;65(2):303-313.
9. Yossepowitch O, Thompson RH, Leibovich BC, et al. Positive surgical margins at partial nephrectomy: predictors and oncological outcomes. *J Urol*. 2008;179:6.
10. Emmadi R, Wiley EL. Evaluation of resection margins in breast conservation therapy: the pathology perspective—past, present, and future. *Int J Surg Oncol*. 2012;2012:180259.
11. Zaffino P, Moccia S, De Momi E, Spadea MF. A review on advances in intra-operative imaging for surgery and therapy: imagining the operating room of the future. *Ann Biomed Eng*. 2020;48(8):2171-2191.
12. Hall NC, Povoski SP, Zhang J, Knopp MV, Martin EW Jr. Use of intraoperative nuclear medicine imaging technology: strategy for improved patient management. *Expert Rev Med Devices*. 2013;10(2):149-152.
13. Van Oosterom NN, Rietbergen DDD, Welling MM, et al. Recent advances in nuclear and hybrid detection modalities for image-guided surgery. *Expert Rev Med Devices*. 2019;16(8):711-734.
14. Sweet WH. The uses of nuclear disintegration in the diagnosis and treatment of brain tumor. *N Engl J Med*. 1951;245:875-887.
15. Vallabhajosula S, Killeen RP, Osborne JR. Altered biodistribution of radiopharmaceuticals: role radiochemical – pharmaceutical purity, physiological, and pharmacologic factors. *Semin Nucl Med*. 2010;40:220-241.
16. Gopal BS. Basics of PET Imaging: physics. In: *Chemistry, and Regulations*. Springer-Verlag; 2010. doi:10.1007/978-1-4419-0805-6
17. Islamian JP, Azazrm A, Mahmoudian B, Gharapapagh E. Advances in pinhole and multi-pinhole collimators for single photon emission computed tomography imaging. *World J Nucl Med*. 2015;14(1):3-9.
18. Zanzonico P, Heller S. The intraoperative gamma probe: basic principles and choices available. *Semin Nucl Med*. 2000;30:33-48.
19. Takeuchi W, Suzuki A, Ueno Y, et al. Semiconductor detector-based scanners for nuclear medicine. In: *Perspectives on Nuclear Medicine for Molecular Diagnosis and Integrated Therapy*. Springer; 2016. doi:10.1007/978-4-431-55894-1_4
20. Scopinaro F, Pani R, Soluri A, et al. Detection of sentinel node in breast cancer: pilot study with the imaging probe. *Tumori*. 2000;86:329-331.
21. Valk PE, Bailey DL, Townsend DW, Maisey MN. *Positron Emission Tomography: Basic Science and Clinical Practice*. Springer-Verlag London Ltd; 2003:41-67.
22. Mao R, Zhang L, Zhu R-Y. LSO/LYSO crystals for future HEP experiments. *J Phys: Conf Ser*. 2011;293(1):012004.
23. Raylman RR, Wahl RL. Evaluation of ion-implanted-silicon detectors for use in intraoperative positron-sensitive probes. *Med Phys*. 1996;23(11):1889-1895.
24. Zanzonico P, Heller S. The intraoperative gamma probe: basic principles and choices available. *Semin Nucl Med*. 2000;30(1):33-48.
25. Chen X. *Molecular Imaging Probes for Cancer Research*. Scientific Publishing Co. Pte. Ltd; 2000:596224.
26. Mariani G, Giuliano AE, Strauss HW. *Radioguided Surgery: A Comprehensive Team Approach*. Springer-Verlag; 2008. doi:10.1007/978-0-387-38327-9
27. Crystal Photonics. Criteria for Gamma Probe Systems. Crystal Photonics GmbH, Germany, 2018. Available at: https://crystal-photonics.com/enu/products/control_unit-criteria–enu.htm
28. Itikawa E, Santos LA, Trevisan AC, et al. Characterization of resolution, sensitivity, and shielding of a gamma-probe for sentinel lymph node localization: an experimental study. *Nucl Med Commun*. 2017;38(10):837-842.
29. Bombardieri E, et al., Sonde intraoperatorie per chirurgia radioguidataprotocollo per il controllo di qualita. Italian Association of Medical Physics (AIFM), Italian Association of Nuclear Medicine (AIMN), Italian Group for Radioguided Surgery and ImmunoScintigraphy (GISCRIS), and National Operative Breast Cancer Force (FONCAM), eds. March 6, 2001. Available in Italian at: http://www.aifm.it; keyword "intraoperatorie"
30. NEMA Standards Publication NU 3-2004., Performance Measurements and Quality Control Guidelines for Non-Imaging Intraoperative Gamma Probes. Copyright 2004 by the National Electrical Manufacturers Association. Available at: www.nema.org
31. Soluri A, Pani R. Italian National Research Council (CNR). Miniaturized gamma camera with very high spatial resolution. Italian patent RM97A000233; US patent 6 242 744 B1. 1997.
32. Soluri A, Scafè R, Falcini F, et al. Mammotome breast cancer biopsy: combined guide with x-ray stereotaxis and imaging probe. *Nucl Instrum Methods A*. 2003;497:122-128.
33. Narita H, Kawaida Y, Ooshita T, et al. Evaluation of efficiency of a multi-crystal scintillation camera Digirad imager using a solid state detector. *Kaku Igaku*. 2001;38:355-362.
34. Abe A, Takahashi N, Lee J, et al. Performance evaluation of a handheld, semiconductor (CdZnTe)-based gamma camera. *Eur J Nucl Med Mol Imaging*. 2003;30:805-811.
35. Spadola S, Verdier MA, Pinot L, et al. Design optimization and performances of an intraoperative positron imaging probe for radioguided cancer surgery. *JINST*. 2016;11:P12019.
36. Spadola S. *Development and Evaluation of an Intraoperative Beta Imaging Probe for Radio-Guided Solid Tumor Surgery*. Medical Physics Université Paris Saclay (COmUE); 2016.
37. D'Errico G, Scafé R, Soluri A, et al. One-inch field of view imaging probe for breast cancer sentinel node location. *Nucl Instrum Methods Phys Res A*. 2003;497:105-109.
38. Gonzalez-Montoro A, Gonzalez AJ, Pourashraf S, et al. Evolution of PET detectors and event positioning algorithms using monolithic scintillation crystals. *IEEE Trans Radiat Plasma Med Sci*. 2021;5(3):282-305.
39. Pitre S, Ménard L, Ricard M, et al. A handheld imaging probe for radio-guided surgery: physical performance and preliminary clinical experience. *Eur J Nucl Med Mol Imaging*. 2003;30:339-343.
40. Orcal K, Dag A, Turkmenoglu O, et al. Radioguided occult lesion localization versus wire-guided localization for non-palpable breast lesions: randomized controlled trial. *Clinics*. 2011;66(6):1003-1007.
41. Sanchez-Gonzalez JV, Ardavín JP, Vera-Donoso C, et al. Re-Roll: a new tool in the surgical treatment of non-exophytic small renal tumors. Application of the radio-guided occult lesion localization (ROLL) technique for renal lumpectomy (RE-ROLL). *Eur Urolo Suppl*. 2018;17(13):e2771.
42. Betancourt JA, Vera Donoso C, Martinez-Sarmiento M, et al. Application of the radio-guided occult lesion localization technique for renal lumpectomy: from the laboratory to the patient. *Clin Nucl Med*. 2017;42(11):e467-e468.
43. Collamati F, Bocci V, Castellucci P, et al. Radioguided surgery with β radiation: a novel application with Ga^{68}. *Sci Rep*. 2018;8:16171.
44. Piert M, Burian M, Meisetschläger G, et al. Positron detection for the intraoperative localisation of cancer deposits. *Eur J Nucl Med Mol Imaging*. 2007;34(10):1534-1544.

45. Franc BL, Mari C, Johnson D, Leong SP. The role of a positron- and high-energy gamma photon probe in intraoperative localization of recurrent melanoma. *Clin Nucl Med*. 2004;30(12):787-791.
46. Berger MJ, Coursey JS, Zucker MA, Chang J, et al. *Stopping-Power & Range Tables for Electrons, Protons, and Helium Ions*. NISTIR; 2017:4999. doi:10.18434/T4NC7P
47. Bonzom S, Menard L, Pitre S, et al. An intraoperative beta probe dedicated to glioma surgery: design and feasibility study. *IEEE Trans Nucl Sci*. 2007;54(1):30–41.
48. Yamamoto S, Matsumoto K, Sakamoto S, et al. An intraoperative positron probe with background rejection capability for FDG-guided surgery. *Ann Nucl Med*. 2005;19:23-28.
49. Raylman RR, Fisher SJ, Brown RS, Ethier SP, Wahl RL. Fluorine-18-fluorodeoxyglucose-guided breast cancer surgery with a positron-sensitive probe: validation in preclinical studies. *J Nucl Med*. 1995;36:1869-1874.
50. Gulec SA, Daghighian F, Essner R. Clinical utility of PET-probe in oncologic surgery (abstract). *Ann Surg Oncol*. 2005;12(suppl):S10.
51. Daghighian F, Mazziotta JC, Hoffman EJ, et al. Intraoperative beta probe: a device for detecting tissue labeled with positron or electron emitting isotopes during surgery. *Med Phys*. 1994;21(1):153-157.
52. Russomando A, Schiariti M, Bocci V, et al. The β-radio-guided surgery: method to estimate the minimum injectable activity from ex-vivo test. *Phys Med*. 2019;58:114-120.
53. Cremonesi M, Ferrari M, Bodei L, Tosi G, Paganelli G. Dosimetry in peptide radionuclide receptor therapy. *J Nucl Med*. 2006;47(9):1467-1475.
54. Camillocci ES, Bellini F, Bocci V, et al. Polycrystalline paraterphenyl scintillator adopted in a β-detecting probe for radio-guided surgery. *J Phys Conf Ser*. 2015;620(1):012009.
55. Raylman R. Performance of a dual, solid-state intraoperative probe system with 18F, ^{99}mTc, and ^{111}In. *J Nucl Med*. 2001;42(2):352-360.
56. Raylman RR. Performance of a dual solid state intraoperative probe system with 18F, 99mTc, and 111In. *J Nucl Med*. 2001;42:352-360.
57. Daghighian F, Mazziotta JC, Hoffman EJ, et al. Intraoperative beta probe: a device for detecting tissue labeled with positron or electron emitting isotopes during surgery. *Med Phys*. 1994;21(1):153-157.
58. Grimm J. Cerenkov luminescence imaging. In: *Imaging and Visualization in the Modern Operating Room*. Springer; 2015. ISBN 978-1-4939-2325-0.
59. Ruggiero A, Holland JP, Lewis JS, Grimm J. Cerenkov luminescence imaging of medical isotopes. *J Nucl Med*. 2010;51(7):1123-1130.
60. Zhang R, Fox CJ, Glaser AK, Gladstone DJ, Pogue BW. Superficial dosimetry imaging of Cherenkov emission in electron beam radiotherapy of phantoms. *Phys Med Biol*. 2013;58(16):5477.
61. Ciarrocchi E, Belcari N, Guerra AD, et al. Cherenkov luminescence measurements with digital silicon photomultipliers: a feasibility study. *EJNMMI Phys*. 2015;2(1):32.
62. Zhang L, Neves L, Lundeen JS, Walmsley IA. A characterization of the single-photon sensitivity of an electron multiplying charge-coupled device. *J Phys B Atomic Mol Optical Phys*. 2009;42(11):114011.
63. Lewis M, Kodibagkar VD, Öz OK, Mason RP. On the potential for molecular imaging with Cerenkov luminescence. *Opt Lett*. 2010;35(23):3889-3891.
64. Robbins M, Hadwen B. The noise performance of electron multiplying charge-coupled devices. *Electron Devices IEEE Trans*. 2003;50(5):1227-1232.
65. Faruqi AR, McMullan G. Direct imaging detectors for electron microscopy. *Nucl Meth Phys Research A*. 2018;878:180-190.
66. Walrand S, Flux GD, Konijnenberg MW, et al. Dosimetry of yttrium-labelled radiopharmaceuticals for internal therapy: 86Y or 90Y imaging? *Eur J Nuclear Med Mol Imaging*. 2011;38(1):57-68.
67. Hu H, Cao X, Kang F, et al. Feasibility study of novel endoscopic Cerenkov luminescence imaging system in detecting and quantifying gastrointestinal disease: first human results. *Eur Radiol*. 2015;25(6):1814-1822.
68. Liu H, Carpenter CM, Jiang H, et al. Intraoperative imaging of tumors using Cerenkov luminescence endoscopy: a feasibility experimental study. *J Nucl Med*. 2012;53(10):1579-1584.
69. Robertson R, Germanos MS, Manfredi MG, et al. Multimodal imaging with 18F-FDG PET and Cerenkov luminescence imaging after MLN4924 treatment in a human lymphoma xenograft model. *J Nucl Med*. 2011;52:1764-1769.
70. Holland JP, Normand G, Ruggiero A, Lewis JS, Grimm J. Intraoperative imaging of positron emission tomographic radiotracers using Cerenkov luminescence emissions. *Mol Imaging*. 2011;10:1-3.
71. Renata M, Tran TA, Axelsson J. 68Ga-labeled superparamagnetic iron oxide nanoparticles (SPIONs) for multi-modality PET/MR/Cherenkov luminescence imaging of sentinel lymph nodes. *Am J Nucl Med Mol Imaging*. 2014;4(1):60-69.
72. Maloney BWW, McClatchy DM, Pogue BW. Review of methods for intraoperative margin detection for breast conserving surgery. *J Biomed Opt*. 2018;23(10):100901.
73. Burrin JM. Fluorescent probes. *New Techniques in Metabolic Bone Disease*. 1990.
74. Alford R, Simpson HM, Duberman J. Toxicity of organic fluorophores used in molecular imaging: literature review. *Mol Imaging*. 2009;8(6):7290.
75. Forero-Shelton M. Peering into cells at high resolution just got easier. *Nat Methods*. 2019;16(4):293-294.
76. Datta R. *Label-Free Fluorescence Lifetime Imaging Microscopy (FLIM) to Study Metabolism and Oxidative Stress in Biological Systems*. UC Irvine; 2016. ProQuest ID: Datta_uci_0030D_14205. Merritt ID: ark:/13030/m5673269.
77. Das S, Thorek DL, Grimm J. Cerenkov imaging. *Adv Cancer Res*. 2014;124:213-234.
78. Medipix4 collaboration., Copyright 2022 by CERN. Available at: https://medipix.web.cern.ch/medipix4
79. Moffatt-Bruce s D, Povoski SP, Sharif S, et al. A novel approach to positron emission tomography in lung cancer. *Ann Thorac Surg*. 2008;86(4):1355-1357.
80. Arabi H, Zaidi H. Applications of artificial intelligence and deep learning in molecular imaging and radiotherapy. *Eur J Hybrid Imaging*. 2020;4(17):00086-00088.
81. Seifert R, Weber M, Kocakavuk E, Rischpler C, Kersting D. Artificial intelligence and machine learning in nuclear medicine: future perspectives. *Semin Nucl Med*. 2021;51(2):170-177.
82. You C, Yang Q, Shan H, et al. Structurally-sensitive multi-scale deep neural network for low-dose CT denoising. *IEEE Access*. 2018;6:41839-41855.
83. You C, Zhao R, Liu F, et al. Class-Aware Generative Adversarial Transformers for Medical Image Segmentation. 2022. arXiv:2201.10737v2.
84. Kim S, Yoon B, Lim J-T, Kim M. Data-driven signal–noise classification for microseismic data using machine learning. *Energies*. 2021;14(5):1499.
85. You C, Yang L, Zhang Y, Wang G. Low-dose CT via deep CNN with skip connection and network in network. Proc. of SPIE. 11113 111131W-1. 2022.
86. Lyu Q, You C, Shan H, Zhang Y, Wang G. Super-Resolution MRI and CT Through GAN-CIRCLE. Proc. of SPIE. 11113 111130X-1. 2019.
87. Guha I, Nadeem SA, You C, et al. Deep learning based high-resolution reconstruction of trabecular bone microstructures

from low-resolution CT scans using GAN-CIRCLE. *Proc SPIE Int Soc Opt Eng*. 2020;11317:113170U.
88. You C, Li G, Zhang Y, et al. CT super-resolution GAN constrained by the identical, residual, and cycle learning ensemble (GAN-CIRCLE). *IEEE Trans Med Sci*. 2020;39(1):188-203.
89. You C, et al., Interpretable and annotation-efficient learning for medical image computing. 5th International Workshop, LABELS 2020, Held in Conjunction with MICCAI 2020, Lima, Peru, October 4–8, 2020, Proceedings: 155–163
90. You C, Zhao R, Staib L, Duncan JS. Momentum Contrastive Voxel-wise Representation Learning for Semi-supervised Volumetric Medical Image Segmentation. 2022. arXiv:2105.07059v4.
91. You C, Zhou Y, Zhao R, et al. SimCVD: Simple Contrastive Voxel-Wise Representation Distillation for Semi-Supervised Medical Image Segmentation. 2022. arXiv:2108.06227v4.
92. Halicek M, Little JV, Wang X, et al. Tumor margin classification of head and neck cancer using hyperspectral imaging and convolutional neural networks. *Proc SPIE Int Soc Opt Eng*. 2018;10576:1057605. PMC6149520.
93. Cakmakci D, Karakaslar EO, Ruhland E, et al. Machine learning assisted intraoperative assessment of brain tumor margins using HRMAS NMR spectroscopy. *PLoS Comput Biol*. 2020;16(11):e1008184.
94. Unger J, Hebisch C, Phipps JE, et al. Real-time diagnosis and visualization of tumor margins in excised breast specimens using fluorescence lifetime imaging and machine learning. *Biomed Opt Express*. 2020;11(3):1216-1230.
95. Yang L, Ghosh RP, Franklin JM, et al. NuSeT: a deep learning tool for reliably separating and analyzing crowded cells. *PLoS Comput Biol*. 2020;16(9):e1008193.
96. Strong VE, Galanis CJ, Riedl CC, et al. Portable PET probes are a novel tool for intraoperative localization of tumor deposits. *Ann Surg Innov Res*. 2009;3:2.
97. Camillocci ES, Baroni G, Bellini F, et al. A novel radioguided surgery technique exploiting β^- decays. *Sci Rep*. 2014;4:4401.
98. Tanha K, Pashazadeh AM, Pogue BW. Review of biomedical Čerenkov luminescence imaging applications. *Biomed Opt Express*. 2015;6(8):3053-3065.
99. Veronesi U, Galimberti V, Mariani L, et al. Sentinel node biopsy in breast cancer: early results in 953 patients with negative sentinel node biopsy and no axillary dissection. *Eur J Cancer*. 2005;41:197-198.
100. Motomura K, Noguchi A, Hashizume T, et al. Usefulness of a solid state gamma camera for sentinel node identification in patients with breast cancer. *J Surg Oncol*. 2005;89:12-17.
101. Vermeeren L, Valdés Olmos RA, Meinhardt W, Horenblas S. Intraoperative imaging for sentinel node identification prostate carcinoma: its use in combination with other techniques. *J Nucl Med*. 2011;52(5):741-744.
102. Brawley OW. Trends in prostate cancer in the united states. *J Natl Cancer Inst*. 2012;45:152-156.
103. Heidenreich A, Bellmunt J, Bolla M, et al. EAU guidelines on prostate cancer. Part 1: Screening, diagnosis, and treatment of clinically localized disease. *Eur Urol*. 2011;59(1):61-71.
104. American Society of Clinical Oncology (ASCO). Liver Cancer: Statistics. 2021. https://www.cancer.net/cancer-types/liver-cancer/statistics
105. Perez-Ardavin J, Sanchez-Gonzalez JV, Martinez-Sarmiento M, et al. Surgical treatment of completely endophytic renal tumor: a systematic review. *Curr Urol Rep*. 2019;20(1):3.

How to cite this article: Gonzalez-Montoro A, Vera-Donoso CD, Konstantinou G, et al. Nuclear-medicine probes: Where we are and where we are going. *Med Phys*. 2022;49:4372-4390.
https://doi.org/10.1002/mp.15690